Carbon 169 (2020) 349–356

Contents lists available at ScienceDirect

Carbon

journal homepage: www.elsevier.com/locate/carbon

Research Article

Reconstructing the fractal clusters of detonation nanodiamonds from small-angle X-ray scattering

Piotr Kowalczyk [a, *], Elda-Zoraida Piña-Salazar [b], Jacob Judas Kain Kirkensgaard [c], Artur P. Terzyk [d], Ryusuke Futamura [e], Takuya Hayashi [f], Eiji Ōsawa [g], Katsumi Kaneko [b], Alina Ciach [h]

[a] College of Science, Health, Engineering and Education, Murdoch University, WA, 6150, Australia
[b] Research Initiative for Supra-Materials, Shinshu University, Nagano, 380-8553, Japan
[c] Deptartment of Food Science, University of Copenhagen, 1958, Frederiksberg, Denmark
[d] Physicochemistry of Carbon Materials Research Group, Faculty of Chemistry, N. Copernicus University in Toruń, 7 Gagarin St., 87-100, Toruń, Poland
[e] Department of Materials Chemistry, Faculty of Engineering, Shinshu University, Nagano, 380-8553, Japan
[f] Department of Electrical Engineering, Shinshu University, Nagano, 380-8553, Japan
[g] Nano-Carbon Research Institute, Ltd., Ueda, Nagano, 386-8567, Japan
[h] Institute of Physical Chemistry, Polish Academy of Sciences, Kasprzaka 44/52, 01-224, Warszawa, Poland

ARTICLE INFO

Article history:
Received 5 June 2020
Received in revised form
31 July 2020
Accepted 2 August 2020
Available online 5 August 2020

Keywords:
Detonation nanodiamonds
Small-angle X-ray scattering
High-resolution transmission electron microscopy
Diffusion-limited aggregation
Radius of gyration
Monte Carlo simulations

ABSTRACT

Detonation nanodiamonds (DND) form fractal-like aggregates composed of polydisperse DND particles. We present a novel methodology for the visualisation and characterisation of fractal clusters of DND from one-dimensional small-angle X-ray scattering (SAXS) intensity. The fractal nature and polydispersity of DND are modelled by combining a diffusion-limited aggregation (DLA) process implemented in Monte Carlo simulations with the distribution of DND sizes measured from high-resolution transmission electron microscopy. The radius of gyration (42–44 nm), aggregation number (850–1150), and the maximum dimension (226–242 nm) of DND fractal clusters were obtained from the fitting of the synchrotron-based SAXS data (q~0.11–4.75 1/nm) measured for two samples of commercialized DND powders by the developed theoretical model.

1. Introduction

Since the discovery of nanodiamond particles in detonation soot (DND) [1–4], a wide range of potential applications of DND in drug delivery, gene therapy, bioimaging, tissue engineering, photonic, spintronic and nanocomposites have been proposed [5–7]. A major weakness of the currently produced DND is their polydispersity (typical diameters between 3 and 8 nm) and complex structure of tightly bound irregular core aggregates [8–12]. The control of the purity, surface chemistry, polydispersity, and aggregation of DND particles is crucial for the realization of their potential applications. Therefore, we must develop reliable methods for the characterisation of individual DND particles as well as their cluster aggregates over the volume of the sample which is not directly measurable in a single experiment.

The three-dimensional (3D) reconstruction of DND clusters formed in powders and liquid solutions of DND aggregates from a knowledge of limited experimental information is an intriguing inverse problem [9,12–17]. Small angle X-ray scattering (SAXS) and small angle neutron scattering (SANS) investigations are expected to yield information on the structural characteristics of DND clusters, such as radius of gyration, maximum size and mass fractal dimension [18]. However, the 3D reconstruction and visualisation of DND clusters topology from one-dimensional scattering intensity is a nonunique and nontrivial problem [19–22]. The goal of the reconstruction process is to find the most probable "realistic" structures of DND clusters (in a statistical sense) from a database of model DND clusters (known also as the ensemble-type approach)

* Corresponding author.
E-mail address: P.Kowalczyk@murdoch.edu.au (P. Kowalczyk).

https://doi.org/10.1016/j.carbon.2020.08.003
0008-6223/

[19]. The postulated mechanism of DND aggregation (cluster level) and the experimental information about DND polydispersity (particle level) should be included in the process of generation of the model DND clusters. Therefore, we briefly present the most recent findings on the polydispersity of DND particles and their organisation on the scattering cluster level.

Krüger et al. [10] investigated the nature of different aggregation models in DND by combination of high-resolution transmission election microscopy (HR-TEM), scanning electron microscopy (SEM), and dynamic light scattering (DLS). The authors concluded that primary nanodiamond particles with an average diameter of ~4.4 nm (~4–5 nm observed from HR-TEM) aggregate into extremely tight core aggregates (called 'agglutinates') having a diameter range of 100–200 nm [10]. Following Tomchuk et al. [18], the nanodiamond powder is a conglomerate of branched agglutinates of different sizes, ranging from 60 to 200 nm. The fractal nature of DND clusters has been extensively studied in liquid solutions by SANS [9,13,14,16,18]. The scattering power exponent D_m $2.4 < 3.0$ at the scattering cluster level was evaluated for liquid systems with a different concentration of nanodiamond particles [18]. Lebedev et al. [23] investigated multilevel structures of diamond gels by SANS. The existence of branched DND aggregates forming a network of gel with a mass fractal dimension of D_m~2.3–2.4 was evidenced from SANS data. At infinite dilution, the extrapolated value of mass fractal dimension equal to 2.35 ± 0.01 is a clear indication of the branched topology of DND chains [23]. Tomchuk et al. [24] estimated the radius of gyration (R_g) of DND clusters in aqueous solutions from SANS and the Guinier approximation [22]. It was shown that R_g of DND clusters in aqueous solutions depends nonlinearly on the concentration of nanodiamond particles. The maximum R_g ~40 nm was reported for 3 C wt %, whereas the minimum R_g ~18 nm was found for 9 C wt %. In a pioneering work, Tomchuk et al. [9] applied the sequential algorithm by Filippov et al. [25] for the reconstruction of the 3D models of DND clusters from SANS intensity curves measured for DND suspensions. Direct comparison of the theoretical and experimental scattering intensities computed for three different models of DND clusters showed that only polydisperse clusters consisting of polydisperse DND particles were able to correctly describe the experimental SANS intensity data [9]. The size of the model cluster was chosen arbitrary in the range of 100 nm (the aggregation number of about 180 for the mean particle size of 3 nm) to repeat the situation with the concentrated RUDDM (Real-Dzerzhinsk Ltd., Dzerzhinsk, Russia) suspensions showing the most pronounced power-law behaviour at the cluster scattering level over a wide q-interval. Interestingly, the R_g strongly depended on the source of the DND powders as well as their concentrations. For RUDUM, $R_g = 14.2$ nm and $R_g > 40$ nm were obtained for powder and liquid solutions, respectively [9]. For SDNS (Single-digit nanodiamonds, PlasmaChem GmbH, Berlin, Germany) solution of 10 mg/l, $R_g = 20$ nm was reported [9]. On the other hand, the mass fractal dimension of ~2.4 was estimated for different DND samples that indicates that the diffusion limited aggregation (DLA) is the most probable mechanism of DND cluster formation and growth. For DND powder (Gansu Lingyun Nano-Material Co., Ltd., Lanzhou, China), Avdeev et al. [13] reported a value of $R_g > 20$ nm for the fractal aggregates of DND with sizes greater than 40 nm.

The asymptotic value of the fractal dimension estimated for DLA process in three-dimension is 2.5 [26]. The experimental values of the mass fractal dimension of ~2.3–2.4 reported by SANS [18] and branched fractal-like structures observed by HR-TEM images [12,27–29] indicate that DLA is the most probable mechanism of DND aggregations. The absence of any close packed clusters of DND (e.g. hard-sphere cluster phases) is crucial for the formulation of the scattering problem. The common numerical methods used for parametric/non-parametric fitting of SAXS/SANS intensities (e.g. integral equations with the structure factor modelled from the equation of state of hard spheres) or the assumption of scattering from monodisperse particles at infinite dilution (e.g. Guinier approximation) [19–22] are questioned for DND powders or suspensions due to fast aggregation of individual DND particles into branched fractal-like structures [9,13,14,16,18]. Therefore, we believe that incorporation of the fractal nature of polydisperse DND clusters and the interference effects is essential for the formulation of the scattering problem and the estimation of the physically- and statistically-meaningful structural properties of DND clusters from the SAXS data.

In this study, we present a novel approach for characterisation and visualisation of 3D DND clusters by combining HR-TEM microscopic observations [12], DLA sequential algorithm of Filippov et al. [25], and the Galerkin method of weighted residuals [19,20]. The proposed methodology is applied to evaluate the pair distance distribution function, radius of gyration, and maximum dimension of DND clusters from a single one-dimensional synchrotron-based SAXS intensity curve measured for two powder samples of DND. Finally, from the fitting of the synchrotron-based SAXS intensities the most probable 3D structures of DND clusters were selected from a database of computer-generated polydisperse DND clusters.

2. Synchrotron-based small angle X-ray scattering measurements (SAXS)

The SAXS profiles of two samples of detonation nanodiamonds (e.g. ND1 and ND2) were measured in BL8S3 beam line of Aichi Synchrotron Radiation Center in Japan. The presence of trace amounts of metallic constituents on ND1 sample was not detectable by the X-ray photoelectron spectroscopy (XPS) analysis (Fig. 1S in Supporting Information). The wavelength of X-ray is 0.092 nm, and the beam size is 1.0 mm × 0.5 mm. For the detector of SAXS, 2-dimensional imaging plate was used. The 2D scattering data were converted to 1D data with scattering parameter q using FIT2D software. The measured q range is from 0.11 to 4.75 nm^{-1}. Before the measurements, nanodiamonds were inserted in borosilicate glass capillaries (WJM-Glas/Muller GmbH) and heated at 350 °C for 2h under vacuum (<0.1 Pa), and then the capillaries were sealed to prevent from adsorbing moisture. The diameter and thickness of glass capillaries are 0.7 mm and 0.01 mm, respectively.

The corrected SAXS profiles of nanodiamonds $I_{corr}(q)$, which we used for the further analysis, were obtained by following equation,

$$I_{corr}(q) = \frac{I_0}{I_{0,ND}} I_{ND}(q) - \frac{I_0}{I_{0,cap}} I_{cap}(q) \quad (1)$$

where I_0, $I_{0,ND}$ and $I_{0,cap}$ are transmitted X-ray intensity at $q = 0$ without sample, for nanodiamonds in capillary and for empty capillary, respectively. In this equation, $I_{ND}(q)$ and I_{cap} (q) are the experimental raw data for SAXS profiles of nanodiamonds in capillary and empty capillary, respectively.

3. Theory and simulation methodology

3.1. Theory: particle level

On the particle level, we model nanodiamonds as quasi-spherical diamond-like particles. In the first approximation we ignore the presence of the sp^2-hybridized carbon shells and irregularity of nanodiamond particles (e.g. polyhedral shapes, the presence of twin crystals, structural defects and dislocations, etc.). As others, we assume log-normal distribution of nanodiamond

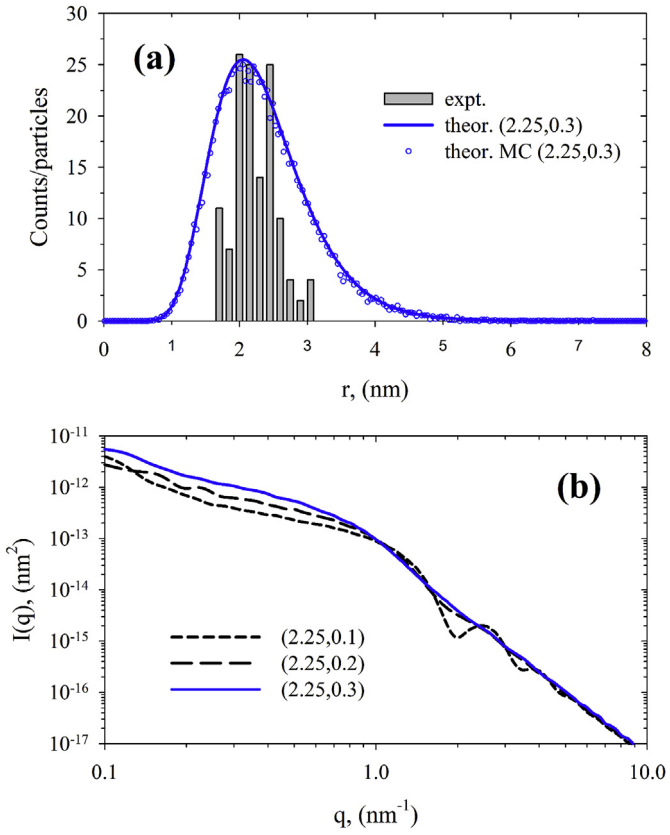

Fig. 1. The polidispersity of detonation nanodiamond particles. (a) Sampling the experimental histogram of nanodiamond sizes collected from HR-TEM images (expt.) [12] from log-normal distribution (theor., $r_0 = 2.25$ nm and $\sigma = 0.3$ nm, eq. (2)) using von Neuman's acceptance-rejection method (theor. MC) [33]. **(b)** Theoretical one-dimensional SAXS intensity curves (eq. (4)) computed for model DLA cluster (R_g ~40 nm) generated from eq. (2) ($r_0 = 2.25$ nm, and $\sigma = 0.1$, 0.2, and 0.3 nm). (A colour version of this figure can be viewed online.)

particle sizes [13,14,30]. Therefore, we describe the experimental HR-TEM histogram of nanodiamond sizes by log-normal distribution function (Fig. 1(a)) [31],

$$n(r) = \frac{1}{r\sigma\sqrt{2\pi}} \cdot exp\left\{ -\frac{1}{2} \frac{\left[ln\left(\frac{r}{r_0}\right)\right]^2}{\sigma^2} \right\} \quad (2)$$

The histogram of nanodiamond sizes collected recently from HR-TEM images [12] approximates the particle size distribution of DND. We note that histogram-based probability density does not drop to zero for the smallest and larges values of r (Fig. 1(a)). The finite number of collected HR-TEM images and the fact that most of the recordings should be distributed around the mean value is the most probable sources of the non-vanishing probabilities at the boundaries. In generation of polydisperse DND clusters, we assume $r_0 = 2.25$ nm and $\sigma = 0.3$ nm in eq. (2) (Fig. 1(a)). The assumed value of r_0 corresponds to the mean size of DND particles that was previously estimated from HR-TEM images [12]. It is consistent with other estimates obtained from scattering techniques [8,10]. Through numerical calculations we find that values of σ ~<0.3 nm in log-normal distribution of DND particle sizes generate oscillations on theoretical SAXS intensities in the experimental q-interval probed by synchrotron, as is shown in Fig. 1(b). In contrast, the experimental synchrotron-based SAXS intensities are smooth over q-range of 0.11–4.75 nm^{-1}, which can be explained by significant polydispersity of DND particles. It is not claimed that $\sigma = 0.3$ nm is unique and optimized value. The log-normal distribution with $r_0 = 2.25$ nm and $\sigma = 0.3$ nm (eq. (2)), is a good representation of the experimental HR-TEM histogram [12], as is shown in Fig. 1(a). At the same time, the SAXS intensity curve computed for model polydisperse DND cluster (R_g~40 nm) generated from log-normal distribution with the above parameters is smooth, as is shown in Fig. 1(b).

3.2. Theory: cluster scattering level

Let us represent the DND sample as a macroscopically isotropic three-dimensional medium composed of aggregates of DND particles with different sizes of clusters. We assume that open fractal-like structure of clusters (see Fig. 2) is formed *via* a DLA process. Once formed, the structure of the clusters is stable and individual DND particles are not moving between different clusters. On the cluster level, we define the theoretical small-angle X-ray scattering intensity by a linear combination of basis functions (also known as the Galerkin method of weighted residuals) [19,20],

$$I_{theor.}(q) = \sum_i \alpha_i \phi_i(q;N) \quad (3)$$

where $q=4\pi\ sin(\theta)/\lambda$ is the modulus of the scattering vector, 2θ is the scattering angle and λ is the wavelength of the incident X-ray beam, $\alpha_i \geq 0$ are weights to be optimized, N denotes the cluster aggregation number, and the intensity $\phi_i(q;\ N)$ is computed for model clusters generated from DLA process implemented in Monte Carlo method via the Debye equation [32],

$$\phi_i(q;N) = \Delta\rho^2 \left(\sum_{i=1}^{N} F^2(q,R_i) + \sum_{i=1}^{N} \times \sum_{j=1, j\neq i}^{N} \left\{ F(q,R_i)F(q,R_j) \left[\frac{sin(qr_{ij})}{qr_{ij}} \right] \right\} \right) \quad (4)$$

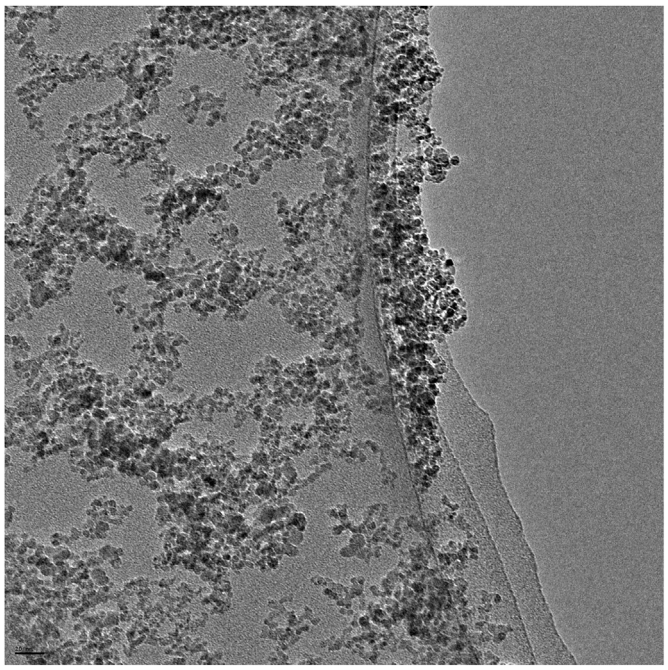

Fig. 2. Aggregates of detonation nanodimon particles. High-resolution transmission electron image of aggregates composed of DND particles. The fractal organisation of the aggregates is clearly visible.

Here $\Delta\rho$ is the excess scattering-length density, R_i and R_j are the radii of the quasi-spherical diamond-like particles with indices i and j, and r_{ij} is their separation in the computer-generated DND cluster. The first term in eq. (4) corresponds to scattering from spherical diamond-like particles, where the form factor is computed from the Rayleigh equation for a homogenous sphere [19,20],

$$F(q,R_i)=\frac{4\pi\rho_0}{q^3}[sin(qR_i)-qR_icos(qR_i)] \quad (5)$$

where ρ_o denotes the density of cubic diamond crystal. The second term in eq. (4) takes into account the interference of the radiation scattered from clusters (e.g. packing effect).

The pair distance distribution function$P(r) = \gamma(r)\cdot r^2$, is computed from the Fourier transform of the theoretical intensity [19,20],

$$P(r)=\frac{r^2}{2\pi^2}\int_0^\infty I_{theor.}(q)q^2\frac{sin(qr)}{qr}dq \quad (6)$$

The radius of gyration R_g is computed from $P(r)$ [19,20],

$$R_g^2=\frac{\int_0^{D_{max}}P(r)\cdot r^2dr}{2\int_0^{D_{max}}P(r)dr} \quad (7)$$

where the maximum dimension of DND clusters, D_{max}, is estimated from condition $P(D_{max})= 0$.

Following the method of least squares, we obtained the values of the unknown vector α in eq. (3) by minimisation of the following quantity with a non-negativity constraint [33],

$$\chi^2(q;\alpha)=\min_{\alpha\geq 0}\sum_i\frac{\left[I_{expt.}(q_i)-I_{theor.}(q_i)\right]^2}{I^2_{expt.}(q_i)} \quad (8)$$

Non-linear minimisation of $\chi^2(q;\alpha)$ was performed using adsorption stochastic algorithm (ASA) that has been developed for solutions of ill-posed problems [34–36].

3.3. Theory: Monte Carlo simulations of nanodiamond clusters

We construct a database consisting of 61 polydisperse 3D clusters of DND particles combining the experimental size distribution function collected from HR-TEM microscopy (Fig. 1(a)) and an in-house DLA Monte Carlo algorithm described by Filippov el al [26]. The radius of gyration of model DND clusters cover the range between 5 nm and 140 nm, which corresponds to the aggregation number of DND particles between 4 and 20000. In our implementation of the DLA Monte Carlo algorithm, a single DND particle (referred also to as a seed) is placed at the centre of a cubic simulation box of side length 700 nm. The radius of the cluster seed and DND particles in the forming cluster are sampled from the experimental histogram using von Neuman's acceptance-rejection sampling method [33], as is shown in Fig. 1(a). Once a cluster seed is placed, we add DND particles into forming cluster iteratively, one by one, with the use of random walk Monte Carlo method [33]. In our implementation of DLA algorithm, we place a DND particle, called a walker, at the randomly selected side length of a simulation box. Next, the walker performs a simple random walk until a termination condition is satisfied. The random walks terminate either when the lifetime of a walker is exceeding the maximum lifetime (in MC steps) or the plastic collision with any of the DND particles in the cluster occurs. The plastic collision

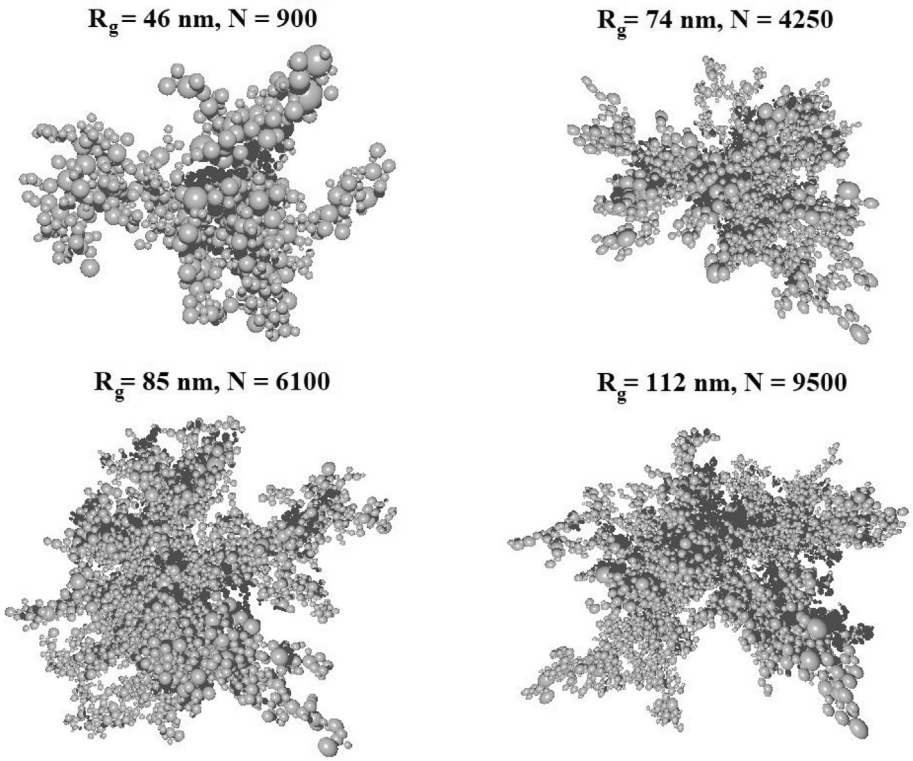

Fig. 3. Polydisperse detonation nanodiamond clusters simulated from DLA Monte Carlo method. Values of radii of gyration (R_g) and aggregation number (N) of polydisperse DND clusters are indicated. The picture is rendered by the *Povray* software [41].

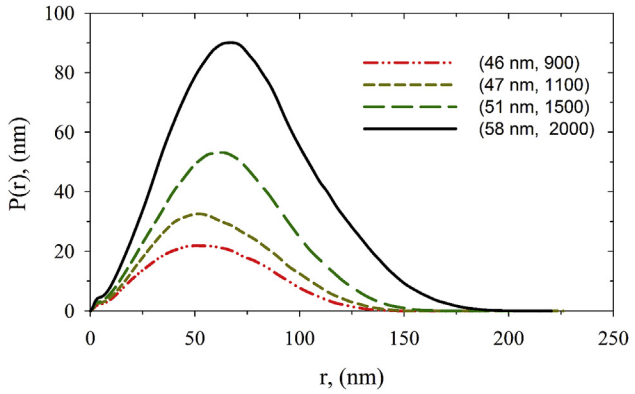

Fig. 4. Pair distance distribution functions computed for polydisperse detonation nanodiamond clusters simulated from DLA Monte Carlo method. Values of radii of gyration and aggregation number of polydisperse DND clusters are shown in brackets, respectively. (A colour version of this figure can be viewed online.)

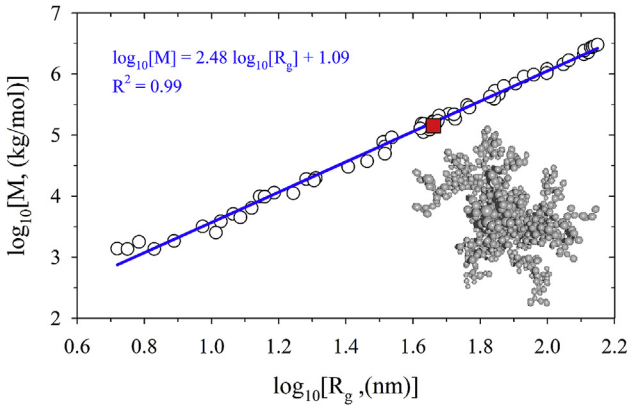

Fig. 5. Fractal-scaling properties. Cluster mass as a function of the radius of gyration of the 3D polydisperse clusters simulated from DLA Monte Carlo method. The inner small panel shows the snapshot of the growing polydisperse branched cluster of DND with aggregation number of 900 and radius of gyration of 46 nm (red square). A mass fractal dimension of polydisperse DLA clusters of 2.48 is determined from the slope of the plot. (A colour version of this figure can be viewed online.)

between the walker and particle occurs when the distance between their surfaces is ~0.325–0.345 nm (e.g. an estimated distance between two DND sp^2-carbon shells in tight cluster). The periodic boundary conditions in *x*, *y*, and *z* directions are used in our implementation [37].

To estimate the mass fractal dimension of the polydisperse computer-generated DND clusters we use the scaling relationship [38],

$$M \sim R_g^{D_m} \tag{9}$$

where $M = \sum_i m_i$, m_i is the mass of a given DND particle, M and R_g denotes the total mass and the radius of gyration of the DND cluster. We compute the radius of gyration from the following equation [39],

$$R_g = \left(\frac{\sum_i m_i (\boldsymbol{r}_i - \boldsymbol{r}_{COM})^2}{\sum_i m_i} \right)^{1/2} \tag{10}$$

where i is the spherical DND particle index in a cluster, $\boldsymbol{r}_i$ is the position of a given a given DND particle, $\boldsymbol{r}_{COM}$ is the position of the center of mass of DND cluster. We estimate D_m from the slope of a plot of $\log_{10} R_g$ versus $\log_{10} M$. Finally, we use eq. (4) to compute theoretical one-dimensional SAXS intensity curves for 61 polydisperse clusters of DND particles from our database.

4. Results and discussion

An example of computer-generated polydisperse DND clusters with corresponding pair distance distribution functions are shown in Figs. 3 and 4, respectively. The fractal morphology of DND clusters with growing elongated branches is clearly visible, however, detailed analysis of the scaling relationship (eq. (9)) is necessary to give deeper insight into self-similarity of model DND clusters. We find that for all generated DND clusters, *P(r)* profiles consist of a single asymmetrical peak (Fig. 4). As expected, the peak on *P(r)* broaden and shift towards larger values of distances as the size of the DND clusters increases. The asymmetry of the *P(r)* with a characteristic tail at longer distances is explained by non-spherical and elongated shapes of DND clusters [21] (Fig. 4). It is worth to point out that the *P(r)* peaks right-side asymmetry were obtained for DND aggregates in suspensions from the indirect Fourier transform method and SANS data [9,18]. Another interesting feature on *P(r)* is poorly visible shoulders at *r* ~2.5 nm that come from the scattering by individual DND particles. These shoulder peaks are smoothed out by the polydispersity of DND particle sizes.

Fig. 5 shows the variation of a radius of gyration with the mass of polydisperse DND clusters computed from eqs. (9) and (10). The good linear correlation for 61 theoretical points is obtained (the Pearson correlation coefficient is equal to 0.99). The estimated mass

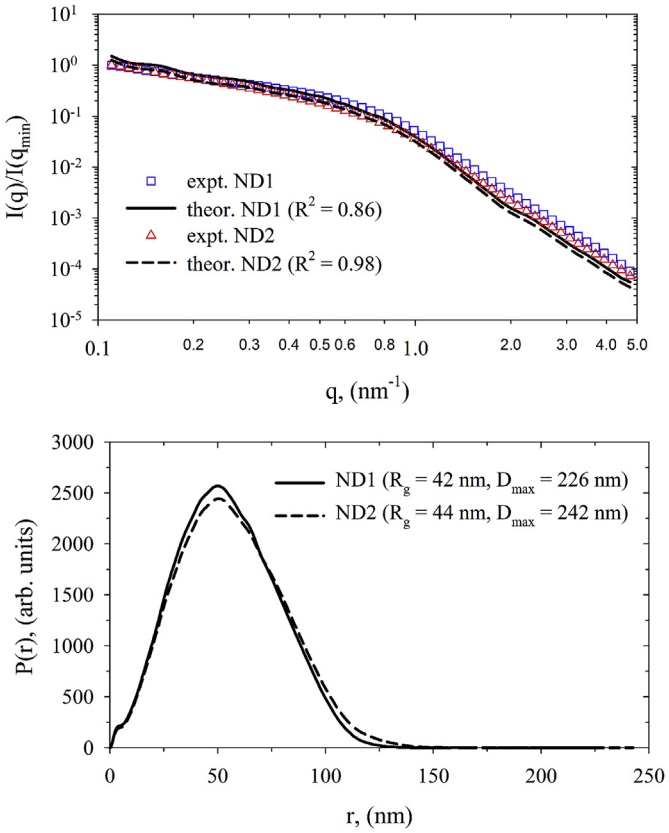

Fig. 6. Experimental validation. Fitting of the experimental one-dimensional synchrotron-based SAXS intensity curves in logarithmic scale by eq. (3) (upper panel) and corresponding pair distance distribution functions (bottom panel) computed from eq. (6). Values of radii of gyration and maximum dimension of polydisperse DND clusters are indicated. (A colour version of this figure can be viewed online.)

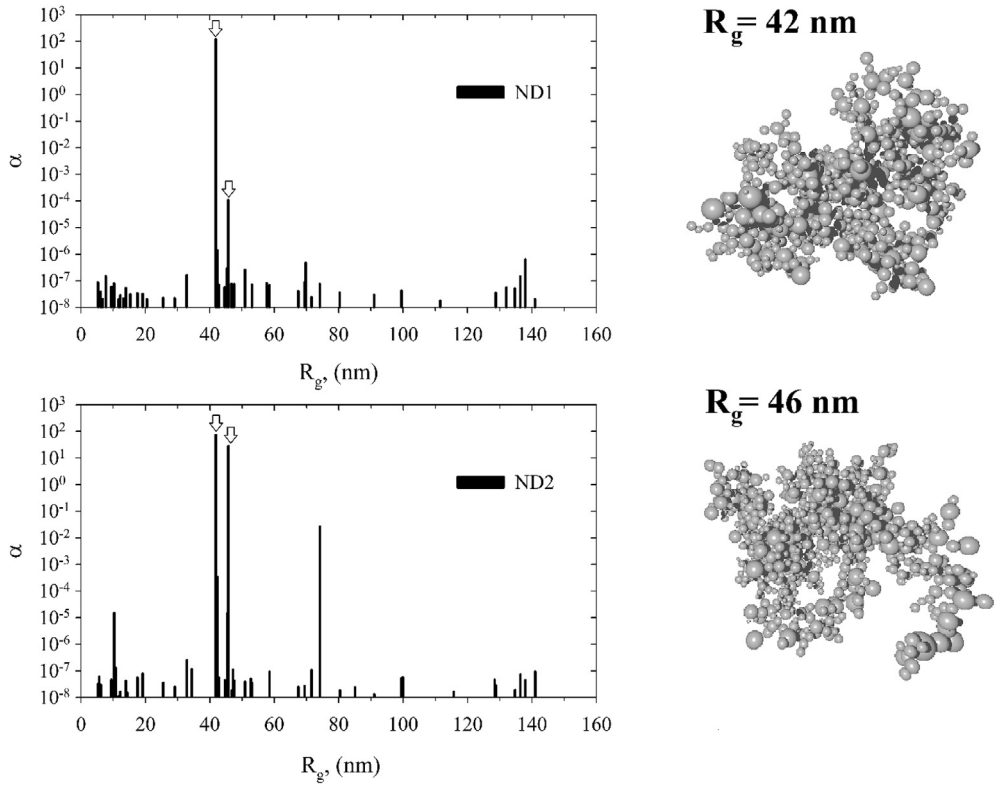

Fig. 7. The most probable fractal-like clusters of detonation nanodiamond particles. Distribution of weights of 61 polydisperse DLA clusters obtained from deconvolution of the one-dimensional synchrotron-based SAXS intensities (eq. (3)) measured for two powder samples of DND (e.g. ND1 and ND2). The right panels display the 3D structure of polydisperse DND clusters with the highest weight contributions. Values of radii of gyration of DND clusters are indicated.

fractal dimension of 2.48 and branched grown pattern of model DND clusters (Fig. 3 and inner panel in Fig. 5) is characteristic for fractal objects growing in the three-dimensional diffusion limited aggregation mode. By comparing the estimated and experimental values of mass fractal dimensions of ~2.3–2.4 reported by SANS [18,40], we conclude that the database of computer-generated polydisperse DND clusters capture the fractal nature of clusters in DND aggregates.

The fitting of the experimental one-dimensional synchrotron-based SAXS intensities measured for two powders of DND by eq. (3) is shown in Fig. 6. The obtained Pearson correlation coefficients are equal to 0.98 and 0.86, indicating good correlation between theory and experiment. We note, however, that theoretical and experimental intensities are shifted for q>~1 nm^{-1}. A possible explanation for this discrepancy is the modelling of DND particles by homogenous diamond-like spheres. Model calculations of form factors showed that the surface reconstruction of nanodiamond particles (e.g. inhomogeneous carbon density profiles at the interface) shift interference peaks on form factors to higher q-values (Figs. 2S–4S in Supporting Information). Therefore, the incorporation of diffusive character of the DND particle interfaces is a promising direction for the improvement of the proposed methodology.

From the fitting of the SAXS data and pair distance distribution functions (Fig. 6), the estimated radius of gyration of DND clusters in the studied powder samples is 42–44 nm. Additionally, we find that two polydisperse DND clusters from our database with the radius of gyration of 42 nm and 46 nm are dominating the distribution of weights in eq. (3), as is shown in Fig. 7. The corresponding aggregation number of DND particles in these clusters is in the range of 850–1150. Following the SANS study of Avdeev et al. [13], the characteristic aggregate size in DND powder is ~40 nm, which is close to our estimation of R_g from synchrotron-based SAXS measurements. According to Krüger et al. [10], the extremely tight core aggregates of DND have a diameter of 100–200 nm. The maximum dimension of DND clusters estimated from pair distance distribution functions is ~226–242 nm, which correlate with the maximum size of core aggregates [10].

To what extent can the distribution of DND particle sizes in computer-generated model DND clusters (Fig. 1(a)) be employed to study aggregation of various samples of DND? How do the carbon sp^3/sp^2-hybridized core-shell structure and non-spherical shape of DND particles impact on DLA process and the computed scattering intensity curves? These questions are difficult to answer. First, the size distribution of DND particles can change with synthesis and processing conditions. Second, the inhomogeneous carbon density profile resulted from the surface reconstruction of DND particles can impact the peak positions on form factors (Figs. 3S–4S in the Supporting Information). These fundamental questions are beyond the scope of this paper. However, we believe that our work represents a new step towards better understanding the structural complexity of DND aggregates.

5. Conclusions

In conclusion, we present a novel methodology for the visualisation and characterisation of fractal clusters of DND from one-dimensional small-angle X-ray scattering intensity. The fractal nature of DND clusters was modelled by DLA process implemented in Monte Carlo simulations. The polydispersity of DND particles in computer-generated clusters was included *via* the histogram of

DND particle sizes collected from HR-TEM images.

From the fractal scaling relation between the radius of gyration and the mass of computer-generated polydisperse DND clusters, we obtained the mass fractal dimension of 2.48. This estimate is close to the experimental mass fractal dimension of DND aggregates of ~2.3–2.4 reported by SANS.

To validate the proposed methodology against experimental data, we measured small-angle X-ray scattering intensities on synchrotron (q~0.11–4.75 1/nm) for two samples of commercialized DND powders. From the reconstructed pair distance distribution functions, we obtained the radius of gyration (42–44 nm), aggregation number (850–1150), and the maximum dimension (226–242 nm) of DND fractal clusters. Furthermore, from the theoretical fitting of synchrotron-based SAXS intensities we found that two polydisperse DND clusters from our database ($R_g = 42$ nm and 46 nm) are the most probable structures of DND clusters. Although the obtained structures of DND clusters are not unique, they appear to be physically sound.

CRediT authorship contribution statement

Piotr Kowalczyk: Writing - original draft. **Elda-Zoraida Piña-Salazar:** Writing - original draft. **Jacob Judas Kain Kirkensgaard:** Writing - original draft. **Artur P. Terzyk:** Writing - original draft. **Ryusuke Futamura:** Writing - original draft. **Takuya Hayashi:** Writing - original draft. **Eiji Ōsawa:** Writing - original draft. **Katsumi Kaneko:** Writing - original draft. **Alina Ciach:** Writing - original draft.

Declaration of competing interest

The authors declare that they have no known competing financial interests or personal relationships that could have appeared to influence the work reported in this paper.

Acknowledgment

The work was partially supported by Grant-in-Aid for Scientific Research (B) (17H03039) and the JST OPERA project. The synchrotron radiation experiments were performed at the BL8S3 beam line of Aichi Synchrotron Radiation Center, Aichi Science & Technology Foundation, Aichi, Japan (Approval No. 201803075).

Appendix A. Supplementary data

Supplementary data to this article can be found online at https://doi.org/10.1016/j.carbon.2020.08.003.

References

[1] V.V. Danilenko, On the history of the discovery of nanodiamond synthesis, Phys. Solid State 46 (2004) 595–599.
[2] A.I. Lyamkin, E.A. Petrov, A.P. Ershov, G.V. Sakovich, A.M. Staver, V.M. Titov, The way to produce diamonds from explosives, Dokl. Akad. Nauk SSSR 302 (1988) 611–613.
[3] N.R. Greiner, D.S. Phillips, J.D. Johnson, F. Volk, Diamonds in detonation soot, Nature 333 (1988) 440–442.
[4] O.A. Shenderova, V.V. Zhirnov, D.W. Brenner, Carbon nanostructures, Crit. Rev. Solid State Mater. Sci. 27 (2002) 227–356.
[5] A. Krüger, Diamond nanoparticles: jewels for chemistry and physics, Adv. Mater. 20 (2008) 2445–2449.
[6] U. Roy, V. Drozd, A. Durygin, J. Rodriguez, P. Barber, V. Atluri, et al., Characterization of nanodiamond-based anti-HIV drug delivery to the brain, Sci. Rep. 8 (2018) 1603.
[7] AYa Vul, O.A. Shenderova (Eds.), Detonation Nanodiamonds. Science and Applications, Pan Stanford Publishing Pte. Ltd., Singapore, 2014.
[8] E. Ōsawa, Recent progress and perspectives in single-digit nanodiamond, Diam. Relat. Mater. 16 (2007) 2018–2022.
[9] O.V. Tomchuk, D.S. Volkov, L.A. Bulavin, A.V. Rogachev, M.A. Proskurnin, M.V. Korobov, et al., Structural characteristics of aqueous dispersions of detonation nanodiamond and their aggregate fractions as revealed by small-angle neutron scattering, J. Phys. Chem. C 119 (2015) 794–802.
[10] A. Krüger, F. Kataoka, M. Ozawa, T. Fujino, Y. Suzuki, A.E. Aleksenskii, et al., Unusually tight aggregation in detonation nanodiamond: identification and disintegration, Carbon 43 (2005) 1722–1730.
[11] E. Ōsawa, Monodisperse single nanodiamond particles, Pure Appl. Chem. 80 (2008) 1365–1379.
[12] E.Z. Pina-Salazar, K. Urita, T. Hayashi, R. Futamura, F. Vallejos-Burgos, J. Włoch, et al., Water adsorption property of hierarchically nanoporous detonation nanodiamonds, Langmuir 33 (2017) 11180–11188.
[13] M.V. Avdeev, N.N. Rozhkova, V.L. Aksenov, V.M. Garamus, R. Willumeit, E. Osawa, Aggregate structure in concentrated liquid dispersions of ultrananocrystalline diamond by small-angle neutron scattering, J. Phys. Chem. C 113 (2009) 9473–9479.
[14] O.V. Tomchuk, M.V. Avdeev, A.E. Aleksenskii, AYa Vul, O.I. Ivankov, V.V. Ryukhtin, et al., Sol-Gel transition in nanodiamond aqueous dispersions by small-angle scattering, J. Phys. Chem. C 123 (2019) 18028–18036.
[15] A.N. Ozerin, T.S. Kurkin, L.A. Ozerina, Dolmatov VYu, X-ray diffraction study of the structure of detonation nanodiamonds, Crystallogr. Rep. 53 (2008) 60–67.
[16] M.V. Avdeev, V.L. Aksenov, O.V. Tomchuk, L.A. Bulavin, V.M. Garamus, E. Ōsawa, The spatial diamond-graphite transition in detonation nanodiamond as revealed by small-angle neutron scattering, J. Phys. Condens. Matter 25 (2013) 445001.
[17] AYa Vul, E.D. Eidelman, A.E. Aleksenskiy, A.V. Shvidchenko, A.T. Dideikin, V.S. Yuferev, et al., Transition sol-gel in nanodiamond hydrosols, Carbon 114 (2017) 242–249.
[18] O.V. Tomchuk, L.A. Bulavin, V.L. Aksenov, M.V. Avdeev, Small-angle scattering in structural Research of nanodiamond dispersions, in: L. Bulavin, L. Xu (Eds.), Modern Problems of the Physics of Liquid Systems, vol. 223, Springer Proceedings in Physics, Cham, 2019, pp. 201–223.
[19] O. Glatter, O. Kratky, Small-Angle X-Ray Scattering, Academic Press, London, 1982.
[20] L.A. Feigin, D.I. Svergun, Structure Analysis by Small-Angle X-Ray and Neutron Scattering, Plenum Press, New York, 1987.
[21] A. Guinier, X-Ray Diffraction: in Crystals, Imperfect Crystals, and Amorphous Bodies, Dover Publications, Inc., New York, 2013.
[22] A. Guinier, G. Fournet, Small-angle Scattering of X-Rays, John Wiley & Sons, Inc., New York, 1955.
[23] V. Lebedev, Y. Kulvelis, A. Kuklin, A. Vul, Neutron study of multilevel structures of diamond gels, Condens. Matter 1 (2016) 1–10.
[24] O.V. Tomchuk, M.V. Avdeev, L.A. Bulavin, V.L. Aksenov, V.M. Garamus, Small-angle neutron scattering by fractal clusters in aqueous dispersions of nanodiamonds, Phys. Part. Nucl. Lett. 8 (2011) 1046–1048.
[25] A.V. Filippov, M. Zurita, D.E. Rosner, Fractal-like aggregates: relation between morphology and physical properties, J. Colloid Interface Sci. 229 (2000) 261–273.
[26] ChM. Sorensen, G.C. Roberts, The prefactor of fractal aggregates, J. Colloid Interface Sci. 186 (1997) 447–452.
[27] A.V. Shvidchenko, E.D. Eidelman, AYa Vul, N.M. Kuznetsov, Stolyarova DYu, S.I. Belousov, et al., Colloids of detonation nanodiamond particles for advanced applications, Adv. Colloid Sci. Interf. Sci. 268 (2019) 64–81.
[28] M. Zeiger, N. Jäckel, M. Aslan, D. Weingarth, V. Presser, Understanding structure and porosity of nanodiamond-derived carbon onions, Carbon 84 (2015) 584–598.
[29] S.L.Y. Chang, P. Reineck, D. Williams, G. Bryant, G. Opletal, S.A. El-Demrdash, et al., Dynamic self-assembly of detonation nanodiamond in water, Nanoscale 12 (2020) 5363–5367.
[30] A.D. Trofimuk, D.V. Muravijova, D.A. Kirilenko, A.V. Shvidchenko, Effective method for obtaining the hydrosols of detonation nanodiamond with particle size < 4 nm, Materials 11 (2018) 1285.
[31] P. Bartlett, R.H. Ottewill, A neutron scattering study of the structure of a bimodal colloidal crystal, J. Chem. Phys. 96 (1992) 3306–3318.
[32] J.S. Pedersen, Determination of size distributions from small-angle scattering data for systems with effective hard-sphere interactions, J. Appl. Crystallogr. 24 (1994) 595–608.
[33] W.H. Press, S.A. Teukolsky, W.T. Vetterling, B.P. Flannery, Numerical Recipes in Fortran, Cambridge University Press, Cambridge, 1992.
[34] P.A. Gauden, P. Kowalczyk, A.P. Terzyk, Toward solving the unstable linear fredholm equation of the first Kind: A new procedure called the adsorption stochastic algorithm (ASA) and its properties, Langmuir 19 (2003) 4253–4268.
[35] P. Kowalczyk, A.P. Terzyk, P.A. Gauden, R. Leboda, E. Szmechtig-Gauden, G. Rychlicki, et al., Estimation of the pore-size distribution function from the nitrogen adsorption isotherm. Comparison of density functional theory and the method of Do and co-workers, Carbon 41 (2003) 1113–1125.
[36] P. Kowalczyk, R. Holyst, H. Tanaka, K. Kaneko, Distribution of carbon nanotube sizes from adsorption measurements and computer simulation, J. Phys. Chem. B 109 (2005) 14659–14666.
[37] M.P. Allen, D.J. Tildesley, Computer Simulation of Liquids, Clarendon Press, Oxford, 1987.
[38] D. Avnir (Ed.), The Fractal Approach to Heterogenous Chemistry: Surfaces Colloids, Polymers, John Wiley & Sons Ltd., Chichester, 1989.
[39] P.Y. Hsiao, Chain morphology, swelling exponent, persistence length, like-charge attraction, and charge distribution around a chain in polyelectrolyte

solutions: effects of salt concentration and ion size studied by molecular dynamics simulations, Macromolecules 39 (2006) 7125–7137.
[40] O.V. Tomchuk, M.V. Avdeev, V.L. Aksenov, V.M. Garamus, L.A. Bulavin, S.N. Ivashevskaya, et al., Comparative structural characterization of the water dispersions of detonation nanodiamonds by small-angle neutron scattering, J. Surf. Invest. 6 (2012) 821–824.
[41] http://www.povray.org/.